Check for updates

Luminescence properties and energy transfer of K₃LuF₆:Tb³⁺,Eu³⁺ multicolor phosphors with a cryolite structure†

Dan Yang,[a] Libing Liao, [ID] *[a] Qingfeng Guo, [ID] *[bc] Lefu Mei,*[a] Haikun Liu,[a] Tianshuai Zhou[a] and Huan Ye[bc]

In recent years, compounds with a cryolite structure have become excellent hosts for luminescent materials. In this paper, Tb³⁺ doped and Tb³⁺/Eu³⁺ co-doped K₃LuF₆ phosphors were prepared *via* a high temperature solid phase sintering method. The XRD, SEM, as well as photoluminescence excitation (PLE) and emission (PL) spectra were measured to investigate the structure and luminescence properties of the as-prepared samples. In the Tb³⁺/Eu³⁺ co-doped K₃LuF₆ samples, both characteristic emission spectra of Tb³⁺ and Eu³⁺ could be observed and the emission color of the K₃LuF₆:0.12Tb³⁺,*x*Eu³⁺ phosphors could be adjusted from green to yellowish pink and the corresponding CIE values could be regulated from (0.2781, 0.5407) in the green area to (0.4331, 0.3556) in the yellowish pink area by controlling the concentration ratio of Eu³⁺/Tb³⁺. In addition, the energy transfer mechanism in Tb³⁺/Eu³⁺ co-doped K₃LuF₆ was calculated to be a quadrupole–quadrupole interaction from Tb³⁺ to Eu³⁺ based on the Dexter's equation.

1. Introduction

Fluoride compounds are potential hosts for luminescent materials due to their suitable chemical stability and excellent luminous properties, and as such, have received a lot of attentions over the past few decades.[1–4] Cryolite is an important kind of fluoride compound, the chemical formula of which can be expressed as M₃NF₆, where M represents monovalent cations such as alkali metal ions (Li⁺, Na⁺, K⁺, Rb⁺) and NH₄⁺, and the sites of N can be occupied by trivalent cations, that is Al³⁺, Y³⁺, Sc³⁺, Ga³⁺, *etc.*[5,6] In addition, the N sites can also be occupied by rare earth ions by isomorphic replacement in the cryolite lattice, such as K₃GaF₆,[7] K₃InF₆,[8] and K₃LuF₆.[9] Since the luminescence behavior of rare earth ions depends on the matrix, it is significant to explore novel cryolite luminescent materials.

On the other hand, multicolor single-phase phosphors occupy an important seat in the field of luminescent materials. In particular, rare-earth ion-doped luminescent materials mixed with blue and UV LEDs are fabricated to produce white light. However, a traditional single-color single-phase strategy

[a]Beijing Key Laboratory of Materials Utilization of Nonmetallic Minerals and Solid Wastes, National Laboratory of Mineral Materials, School of Materials Sciences and Technology, China University of Geosciences, Beijing 100083, China. E-mail: clayl@cugb.edu.cn; mlf@cugb.edu.cn

[b]School of Gemology, China University of Geosciences, Beijing 100083, China

[c]Jewelry and Mineral Materials Laboratory of Experimental Teaching Demonstration Center, Beijing, China

† Electronic supplementary information (ESI) available. See DOI: 10.1039/c8ra10059d

usually requires a complicated synthetic process, multiple excitation wavelengths with different responses of the various dopants to the excitation wavelength and reabsorption of the dopant.[10] Single excitation wavelength excited phosphors with multicolor emissions (cyan-emitting, blue-green-emitting, and blue-red-emitting phosphors) can efficiently avoid the above problems and make it easier to obtain a phosphor with high luminous efficiency, excellent color rendering index (CRI), good thermal and chromatic stability. Accordingly, multicolor single-phase phosphors have received attention over the past few decades.[11–13]

Energy transfer is an important way to realize single-phase multicolor phosphors, which have been investigated in abundant hosts.[14] As we know, energy transfer is achieved by ion pairs from a sensitizer to activator, such as Eu²⁺/Tb³⁺, Ce³⁺/Eu²⁺, Ce³⁺/Dy³⁺, Tb³⁺/Eu³⁺, Er³⁺/Sm³⁺, Tm³⁺/Dy³⁺ and so on.[15–20] Due to ⁵D₀ → ⁷F₂ electronic transitions, Eu³⁺-doped luminescent materials can emit strong red light.[21] Tb³⁺ has been widely used together with Eu³⁺ to produce multicolor emission by means of energy transfer, such as in CaMoO₄:Tb³⁺/Eu³⁺,[22] Ba₂La₃(SiO₄)₃-F:Tb³⁺/Eu³⁺, and[23] Na₂MgSiO₄:Tb³⁺/Eu³⁺.[24] However, until now, there have been no reports on the crystal structure, luminescence properties and energy transfer investigations of multicolor-emitting K₃LuF₆:Tb³⁺,Eu³⁺ phosphors with a cryolite structure.

In the present work, Tb³⁺ and Tb³⁺/Eu³⁺ activated cryolite-type K₃LuF₆ compounds were synthesized in a simple way and the crystal structure and luminescence properties, as well as the energy transfer mechanism between Tb³⁺ and Eu³⁺ in K₃LuF₆

were thoroughly studied. Benefiting from the crystal field environment of the cryolite-type samples, the emission color of K_3LuF_6:Tb^{3+},Eu^{3+} could be continuously regulated from green to yellowish pink by changing the content ratio of Tb^{3+}/Eu^{3+}.

2. Experimental section

2.1. Materials and synthesis

K_3LuF_6:$x$$Tb^{3+}$ ($x = 0.01, 0.03, 005, 0.07, 0.09, 0.10, 0.12$ and 0.13) and K_3LuF_6:$0.12Tb^{3+}$,$x$$Eu^{3+}$ ($x = 0.03, 005, 0.07, 0.10$ and 0.13) phosphors were prepared *via* a high temperature solid-state method. The raw materials included K_2CO_3 (AR), Lu_2O_3 (99.99%), NH_4HF_2 (AR), Eu_2O_3 (99.99%) and Tb_4O_7 (99.99%). Firstly, the raw materials were weighed according to the stoichiometric ratios of the reactions and were then ground in a mortar for nearly 10 min, resulting in a uniform mixture. Considering the loss of fluorine sources at high temperatures, a 30% excess of NH_4HF_2 was required during the weighing process. Secondly, the mixture was moved to a furnace and heated at heating rate of $4°$ min^{-1} and was maintained at 800 °C for 3 h under an argon atmosphere. Finally, the systems were naturally cooled down to room-temperature and evenly reground prior to characterization.

2.2. Characterization

The powder X-ray diffraction (PXRD) measurements of the phosphors were performed using a Bruker Corporation D8 powder X-ray diffractometer (Germany) equipped with a Cu kα radiation source at 0.15406 nm, a tube voltage of 40 kV and a tube current of 40 mA. The step scanning rate used was $8°$ min^{-1} over the 2θ range from $10°$ to $70°$. Morphological analysis of the compounds was carried out using a scanning electron microscope (SEM, JSM-6701F, Hitachi, Japan). The photoluminescence (PL) and photoluminescence excitation behavior were measured using a Hitachi F-4600 fluorescence spectrophotometer at room temperature, with a xenon lamp (400 V, 150 W) acting as the light source.

3. Results and discussion

3.1. Crystal structure

The PXRD patterns of the as-prepared K_3LuF_6:$x$$Tb^{3+}$ ($x = 0.01$, $0.03, 005, 0.07, 0.09, 0.1, 0.12$ and 0.13) and K_3LuF_6:0.12-Tb^{3+},$x$$Eu^{3+}$ ($x = 0.03, 005, 0.07, 0.1$ and 0.13) phosphors are shown in Fig. 1(a) and (b). The standard PXRD pattern of K_3LuF_6 (JCPDS no. 27-467) is shown as a reference. As shown in Fig. 1(a) and (b), all of the PXRD patterns of the as-prepared K_3LuF_6:Tb^{3+}
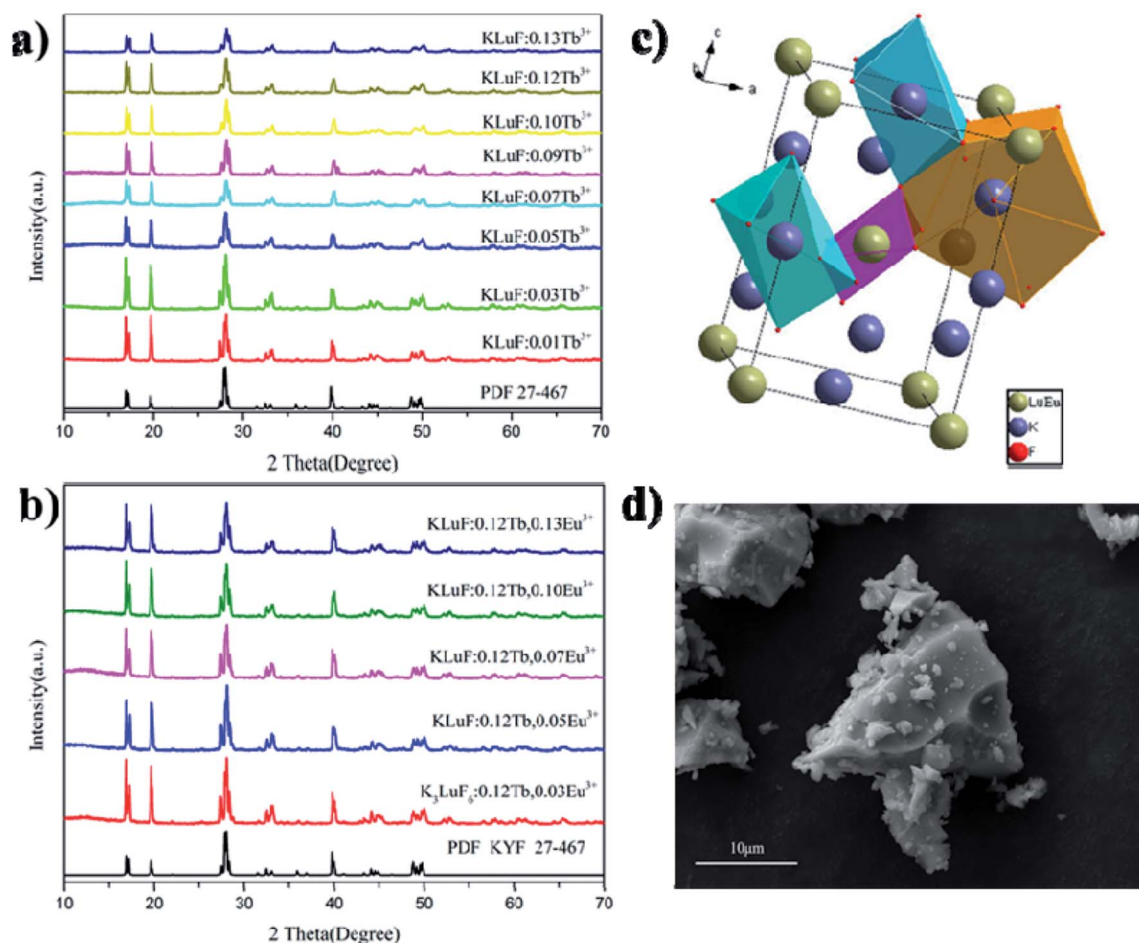

Fig. 1 (a) The PXRD patterns of the as-prepared K_3LuF_6:$x$$Tb^{3+}$ ($x = 0.01, 0.03, 005, 0.07, 0.09, 0.10, 0.12$ and 0.13) and (b) K_3LuF_6:$0.12Tb^{3+}$,$x$$Eu^{3+}$ ($x = 0.03, 005, 0.07, 0.10$ and 0.13) phosphors, (c) the crystal structure of K_3LuF_6, and (d) the SEM image of the K_3LuF_6:$0.12Tb^{3+}$,$0.07Eu^{3+}$ sample.
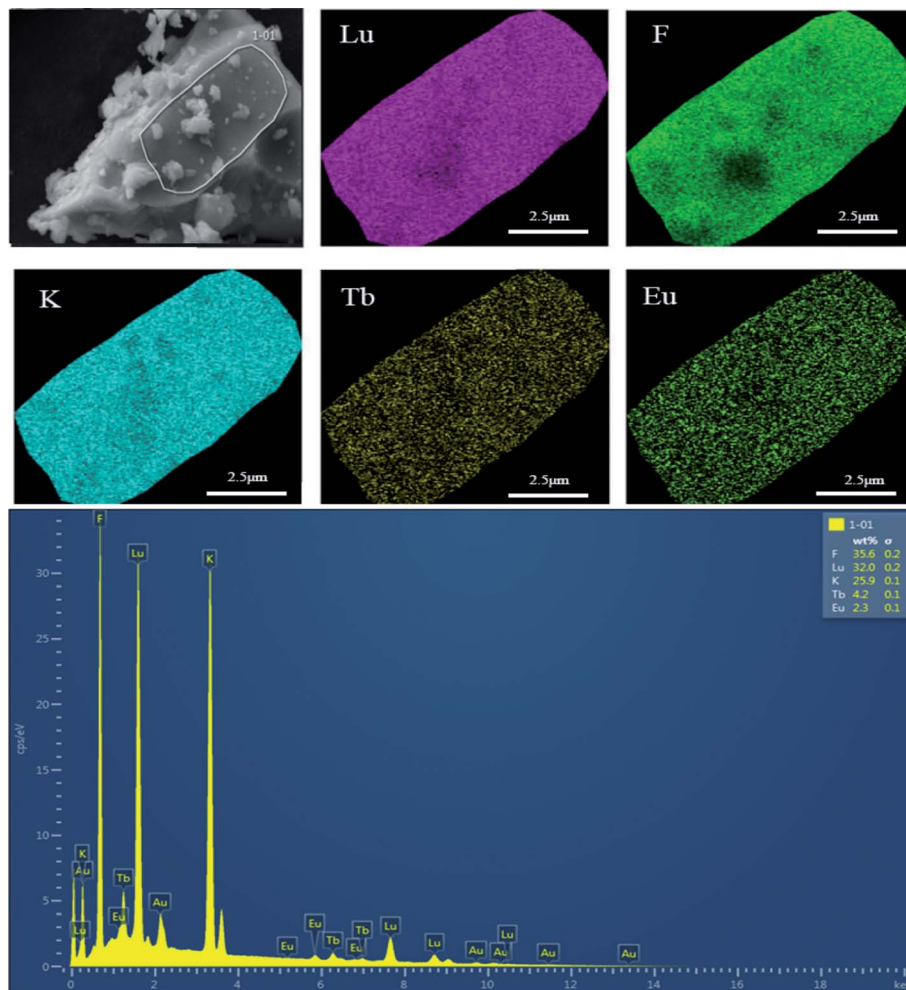
Fig. 2 SEM image, elemental mapping images and EDX spectrum of the K_3LuF_6:0.12Tb^{3+},0.07Eu^{3+} phosphor.

and K_3LuF_6:0.12Tb^{3+},Eu^{3+} samples can be accurately assigned to the standard card of K_3LuF_6, without the appearance of any impurity peaks, which indicates that the introduction of Tb^{3+} and Eu^{3+} in K_3LuF_6 does not bring about any significant changes in the crystal structure. Fig. 1(c) shows the crystal structure of K_3LuF_6, which belongs to a monoclinic phase with a space group of $P2_1/n$. As depicted in Fig. 1(c), the Lu atom coordinates to six F atoms forming [LuF$_6$] octahedra, with the Lu atom in the centre. Two nonequivalent sites for the K atoms can be found in the crystal structure of K_3LuF_6, that is, twelve-coordinated K and six-coordinated K. Based on the charge balance and effective ionic radii, Tb^{3+} and Eu^{3+} were thought to occupy the sites of Lu^{3+}. Fig. 1(d) shows the SEM image of K_3LuF_6:0.12Tb^{3+},0.07Eu^{3+}, which indicates the prepared sample with an irregular shape and the particle size ranges from a few hundred nanometers to dozens of microns (Fig. 2).

The elemental composition and distribution of the prepared K_3LuF_6:0.12Tb^{3+},0.07Eu^{3+} were investigated and the results are shown in Fig. 3. In addition, the elemental composition and distribution of the prepared K_3LuF_6:0.12Tb^{3+},xEu^{3+} (x = 0, 0.03, 0.05, 0.07, 0.10, and 0.13) are shown in Fig. S1–S6,† among which the Au element was introduced to enhance the conductivity of the material during testing. The particles in all the

samples seem like blocks with aggregation. The energy-dispersive X-ray (EDX) spectrum illustrates the existence of elemental K, Lu, F, Tb, and Eu in the sample, except for in the Tb^{3+} single-doped sample. Moreover, the elemental mapping results confirmed that all of the elements in the sample were homogenously distributed over the whole area.

3.2. Photoluminescence properties and energy transfer process

Fig. 3(a) shows the PLE (λ_{em} = 550 nm) and PL (λ_{ex} = 375 nm) spectra of the K_3LuF_6:0.12Tb^{3+} phosphor. As depicted in Fig. 3(a), the PLE spectrum of the K_3LuF_6:0.12Tb^{3+} sample shows typical transitions of Tb^{3+} ranging from 310 to 460 nm, attributed to $^7F_6$–$^5H_7$ (315 nm), $^7F_6$–$^5D_2$ (340 and 351 nm), $^7F_6$–$^5D_4$ (357 nm), $^7F_6$–$^5D_3$ (375 nm), and $^7F_6$–$^5G_6$ (440 nm), respectively. The excitation peak at 375 nm ($^7F_6$–$^5D_3$) is the most intense, matching well with near ultraviolet light LED chips, indicating that this sample has the potential for application in LEDs. When the phosphor was monitored at 375 nm, the PL spectrum of the K_3LuF_6:0.12Tb^{3+} sample exhibited several peaks located at 488/499, 540/550, 586/599, and 624 nm, respectively. These peaks can be assigned as the characteristic
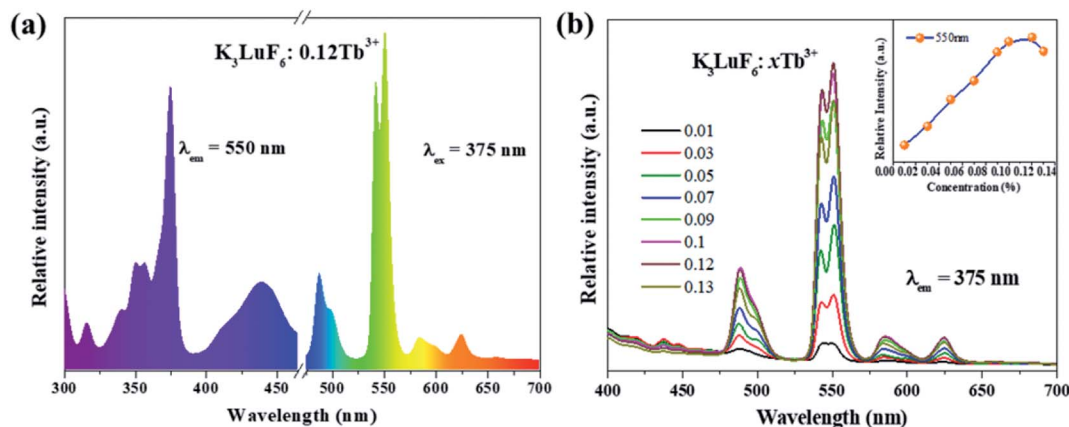
Fig. 3 (a) The photoluminescence excitation (PLE) ($\lambda_{em} = 550$ nm) and emission (PL) ($\lambda_{ex} = 375$ nm) spectra of the $K_3LuF_6:0.12Tb^{3+}$ phosphor, and (b) the emission PL spectra ($\lambda_{ex} = 375$ nm) of the $K_3LuF_6:xTb^{3+}$ ($x = 0.01$, 0.03, 005, 0.07, 0.09, 0.10, 0.12 and 0.13) phosphors. The inset depicts the relative emission-intensity trends for the 550 nm peak ($^5D_4-^7F_3$) in terms of the Tb^{3+} concentration.

emission of $^5D_4-^7F_n$ ($n = 6, 5, 5$ and 3). Fig. 3(b) shows the emission PL spectra of the $K_3LuF_6:xTb^{3+}$ ($x = 0.01$, 0.03, 005, 0.07, 0.09, 0.1, 0.12 and 0.13) phosphors monitored at 375 nm, and the inset depicts the relative emission-intensity trends for the 550 nm peak ($^5D_4-^7F_3$) regarding the Tb^{3+} concentration. Upon 375 nm excitation, all of the PL spectra of the $K_3LuF_6:$-xTb^{3+} samples showed characteristic Tb^{3+} emission peaks, attributed to $J = 6, 5, 4$, and 3. It is well known that the emission intensity of the $^5D_3-^7F_J$ ($J = 6, 5, 4$, and 3) transitions of Tb^{3+} are quenched upon an increase in the Tb^{3+} concentration, ascribed to the cross-relaxation effect regarding the $^5D_3-^7F_J$ levels.[25–27] Meanwhile, the emission intensity for the 550 nm ($^5D_4-^7F_3$) peak increased upon an increase in the concentration of the Tb^{3+} concentration up to $K_3LuF_6:0.12Tb^{3+}$, and then it decreased due to concentration quenching.[28] Thus, the Tb^{3+} doping concentration was fixed at 0.12 (mol) for the co-doping of Tb^{3+} and Eu^{3+} in K_3LuF_6.

In order to further investigate the possibility of energy transfer behavior between Tb^{3+} and Eu^{3+} in K_3LuF_6,

$K_3LuF_6:0.12Tb^{3+},xEu^{3+}$ ($x = 0.03$, 005, 0.07, 0.1 and 0.13) phosphors were prepared. The PLE and PL spectra of the Tb^{3+} and Eu^{3+} single-doped, as well as Tb^{3+}/Eu^{3+} co-doped K_3LuF_6 phosphors are shown in Fig. 4. Under 393 nm excitation, the as-prepared $K_3LuF_6:0.1Eu^{3+}$ sample shows sharp peaks at 579, 590, 613, 624, and 656 nm in Fig. 4(a), which are due to the $^5D_0-^7F_0$, $^5D_0-^7F_1$, $^5D_0-^7F_2$, $^5D_0-^7F_2$, and $^5D_0-^7F_3$ transitions of Eu^{3+}, respectively. In addition, the emission intensity of the peak at 613 nm is the highest among the transitions of Eu^{3+}, as shown in Fig. 4(b). When monitored at 613 nm, the PLE spectrum of $K_3LuF_6:0.1Eu^{3+}$ exhibits a series of sharp excitation bands between 300 and 500 nm, centered at 318, 361, 379, 393, and 414 nm, which can be attributed to the $^7F_0-^5H_5$, $^7F_0-^5D_4$, $^7F_0-^5L_6$, $^7F_0-^5L_7$ and $^7F_0-^5D_3$ transitions, respectively.[29,30] The strongest excitation peak can be obviously observed at 393 nm. The PLE and PL spectra of the $K_3LuF_6:0.12Tb^{3+},0.1Eu^{3+}$ phosphor are illustrated in Fig. 4(b). As shown in Fig. 4(c), when the co-doped sample was excited by near ultraviolet light at 375 nm, both characteristic emission peaks of Tb^{3+} and Eu^{3+} could be
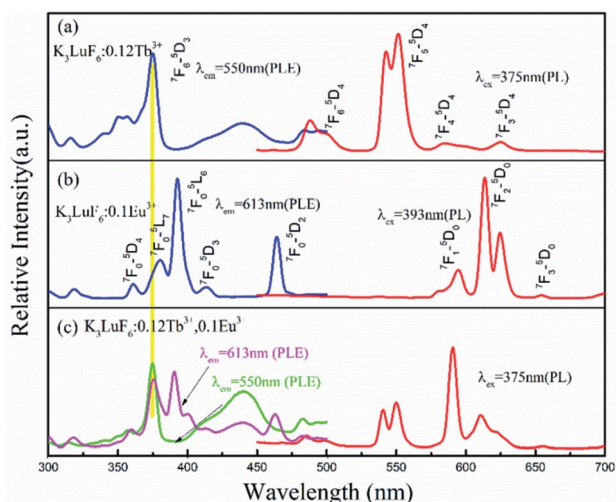

Fig. 4 The PLE and PL spectra of (a) $K_3LuF_6:0.12Tb^{3+}$, (b) $K_3LuF_6:0.1Eu^{3+}$, and (c) $K_3LuF_6:0.12Tb^{3+},0.1Eu^{3+}$.

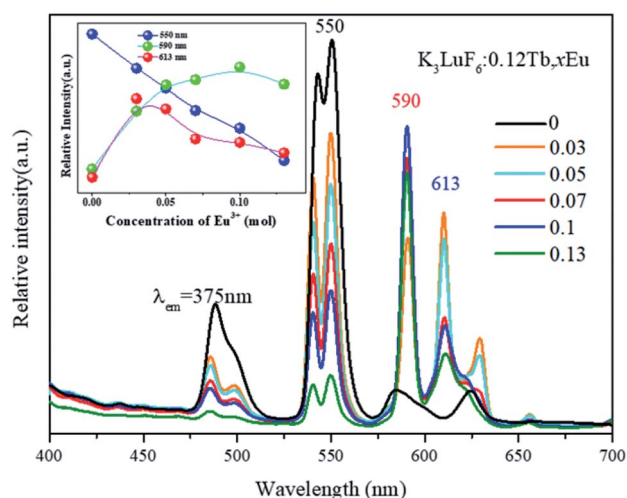**Fig. 5** The PL spectra of $K_3LuF_6:0.12Tb^{3+},xEu^{3+}$ ($x = 0$, 0.03, 005, 0.07, 0.1 and 0.13) under excitation at 375 nm. The inset shows the relative emission intensities at 550, 590, and 613 nm.
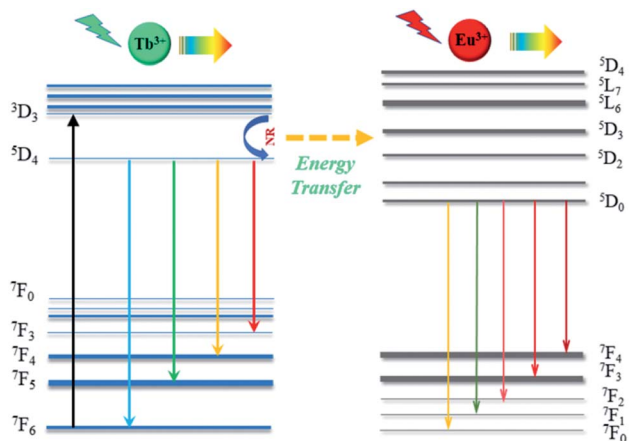
Fig. 6 Energy levels of the possible energy transfer mechanism from Tb^{3+} to Eu^{3+}.

observed in the PL spectrum, indicating that energy transfer may occur between Tb^{3+} and Eu^{3+} in K_3LuF_6. Moreover, when monitored by 613 nm light, which is the typical emission wavelength of Eu^{3+}, the K_3LuF_6:$0.12Tb^{3+}$,$0.1Eu^{3+}$ phosphor showed a characteristic excitation peak (375 nm) of Tb^{3+}, while the peak at 375 nm could not be found in the excitation spectrum. Therefore, energy transfer from Tb^{3+} to Eu^{3+} exists in the K_3LuF_6 host and the emission color for K_3LuF_6:Tb^{3+}/Eu^{3+} can be regulated according to different energy transfer efficiencies by adjusting the ratio of Eu^{3+}/Tb^{3+}.[31] However, when the monitoring light was changed to 550 nm, the excitation spectrum of the co-doped sample did not exhibit the typical Eu^{3+} excitation

peak. Therefore, it could be inferred that the energy transfer process is irreversible in this system.

To further investigate the energy transfer process, the K_3-LuF_6:$0.12Tb^{3+}$,xEu^{3+} ($x = 0$, 0.03, 005, 0.07, 0.1 and 0.13) samples were synthesized using the same method. The PL spectra of K_3LuF_6:$0.12Tb^{3+}$,xEu^{3+} ($x = 0$, 0.03, 0.05, 0.07, 0.1 and 0.13) under the excitation of 375 nm were recorded and the results are shown in Fig. 5. The inset shows the relative emission intensity at 550, 590, and 613 nm, respectively. Upon 375 nm excitation and with increasing Eu^{3+} concentration, the emission intensity of Tb at 550 nm ($^5D_4$–$^7F_3$ transitions) decreases all the time and the emission intensity of Eu^{3+} at 590 nm ($^5D_0$–$^7F_1$ transitions) increases and reaches a maximum at $x = 0.10$, after which the emission intensity decreases, caused by the concentration quenching of Eu^{3+} itself.[32] The results indicate that energy transfer occurs from Tb^{3+} to Eu^{3+} in the K_3LuF_6 host. The emission intensity of Eu^{3+} at 613 nm ($^5D_0$–$^7F_2$ transitions) increases and reaches a maximum at $x = 0.03$, then the emission intensity decreases upon an increase in the Eu^{3+} concentration, which can be ascribed to the concentration quenching of Eu^{3+}.

Fig. 6 shows energy levels of the possible energy transfer mechanism between Tb^{3+} and Eu^{3+}. As depicted in Fig. 6, the Tb^{3+} electrons in the $^7F_6$ ground state energy level can be excited by n-UV light and jump to the $^5D_3$ excited state level. Then, they relax to the $^5D_4$ transition state due to multi-phonon relaxation. As is known, the excited states are not stable, and Tb^{3+} can exhibit green light when the electrons leap back from $^5D_4$ to ^7F_J ($J = 6$, 5, 4, and 3) with non-radiative processes from $^5D_3$ to $^5D_4$.
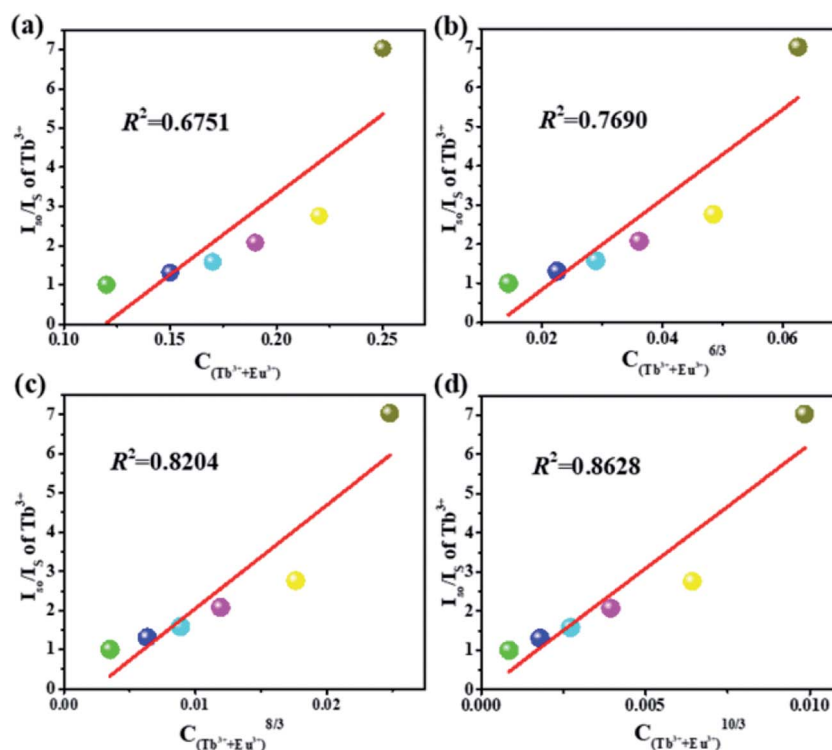

Fig. 7 Dependence of I_{s0}/I_S of Tb^{3+} on (a) C, (b) $C^{6/3}$, (c) $C^{8/3}$ and (d) $C^{10/3}$ for the K_3LuF_6:$0.12Tb^{3+}$,xEu^{3+} ($x = 0$, 0.03, 005, 0.07, 0.1 and 0.13) samples.

Table 1 The CIE chromaticity coordinates of the K_3LuF_6:0.12-Tb^{3+},xEu^{3+} (x = 0, 0.03, 005, 0.07, 0.10 and 0.13) samples under 375 nm excitation

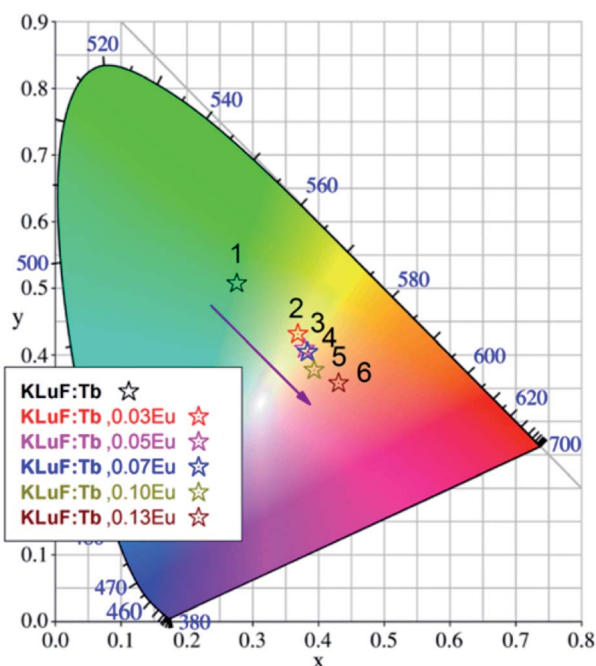| No.	K_3LuF_6:0.12Tb^{3+},xEu^{3+}	(x, y)
1	$x = 0$	(0.2781, 0.5047)
2	$x = 0.03$	(0.3710, 0.4289)
3	$x = 0.05$	(0.3812, 0.4069)
4	$x = 0.07$	(0.3857, 0.4019)
5	$x = 0.10$	(0.3958, 0.3750)
6	$x = 0.13$	(0.4331, 0.3556)

Fig. 8 The CIE chromaticity coordinate diagram of the K_3LuF_6:0.12-Tb^{3+},xEu^{3+} (x = 0, 0.03, 005, 0.07, 0.10 and 0.13) samples under 375 nm excitation.

On the other hand, some Tb^{3+} electrons transfer their energy from the $^5D_4$ (Tb^{3+}) level to the excited state of Eu^{3+} ($^5D_1$ and $^5D_2$) by cross-relaxation, and then the Eu^{3+} ($^5D_1$ and $^5D_2$) electrons relax to the $^5D_0$ level in a non-radiative process, resulting in $^5D_0$–^7F_J (J = 0, 1, 2, 3, and 4) transitions of Eu^{3+}, which produce a red emission color.

In order to further understand the energy transfer mechanism of multi-polar interactions between the Tb and Eu ions in this system, the Dexter equation can be applied, as follows:[33,34]

$$(\eta_{s0}/\eta_s) \propto C^{n/3} \qquad (1)$$

in which η_{s0} is the quantum efficiency of Tb^{3+} in the absence of Eu^{3+} and η_s in the presence of Eu^{3+}, C represents the total concentration of Tb^{3+} and Eu^{3+}, n is a constant value, 3, 6, 8 or 10, corresponding to the exchange, dipole–dipole, dipole–quadrupole and quadrupole–quadrupole interactions, respectively.[35,36] The value of η_0/η_s can be approximately calculated from the ratio of the photoluminescence intensity (I_{s0}/I_s).

Furthermore, Fig. 7 shows the I_{s0}/I_S vs. $C^{n/3}$ (n = 3, 6, 8, or 10) correlation diagram of these phosphors. When n = 10, an optical linear relationship was observed, which corresponds to the quadrupole–quadrupole interaction between Tb^{3+} and Eu^{3+} in K_3LuF_6.

The CIE chromaticity coordinate diagram of the K_3-LuF_6:0.12Tb^{3+},xEu^{3+} (x = 0, 0.03, 005, 0.07, 0.1 and 0.13) phosphors under 375 nm excitation was calculated on the basis of the corresponding emission spectra, which are depicted in Table 1 and Fig. 8. As shown in Table 1 and Fig. 8, the emission color of K_3LuF_6:0.12Tb^{3+},xEu^{3+} can change from green (0.2781, 0.5407) to yellowish pink (0.4331, 0.3556) upon an increase in the concentration of Eu^{3+}. Therefore, K_3LuF_6:0.12Tb^{3+},xEu^{3+} can be efficiently excited by 375 nm as an adjustable luminescence material for use in n-UV LEDs.

4. Conclusions

In summary, single-phase K_3LuF_6:xTb^{3+} (x = 0.01, 0.03, 005, 0.07, 0.09, 0.1, 0.12 and 0.13) and K_3LuF_6:0.12Tb^{3+},xEu^{3+} (x = 0.03, 005, 0.07, 0.1 and 0.13) samples were successfully prepared via a high temperature solid-state phase sintering method. In order to determine the energy transfer mechanism between the Tb^{3+} and Eu^{3+} ions, the photoluminescence properties and decay lifetimes were measured, and the results showed an energy transfer mechanism from Tb^{3+} to Eu^{3+} in K_3LuF_6, determined as a quadrupole–quadrupole interaction. Characteristic emissions for both Tb^{3+} and Eu^{3+} can be observed in the PL spectrum of the co-doped phosphors at an excitation of 375 nm (Tb^{3+}), while the luminescent colors of the K_3-LuF_6:0.12Tb^{3+},xEu^{3+} samples can be regulated by changing the concentration of Eu^{3+}. All of the above results show that the phosphor could be an ideal single-phase multicolor phosphor.

Conflicts of interest

There are no conflicts to declare.

Acknowledgements

References

1 M. Runowski and S. Lis, Synthesis of lanthanide doped CeF_3:Gd^{3+}, Sm^{3+} nanoparticles, exhibiting altered luminescence after hydrothermal post-treatment, *J. Alloys Compd.*, 2016, **661**, 182–189.

2 M. Runowski, J. Marciniak, T. Grzyb, D. Przybylska, A. Shyichuk, B. Barszcz, A. Katrusiak, S. Lis, A. Katrusiak and S. Lis, Lifetime Nanomanometry – High-Pressure Luminescence of Up-converting Lanthanide Nanocrystals-SrF_2:Yb^{3+}, Er^{3+}, *Nanoscale*, 2017, **9**, 16030–16037.

3 L. Qin, P. Q. Cai, C. L. Chen, J. Wang, S. Kim, Y. L. Huang and H. J. Seo, Optical performance of the $Ba_5Al_3F_{19}$:Eu^{2+} blue

phosphors with high thermal stability, *J. Alloys Compd.*, 2018, **738**, 372–378.

4 V. D. Shcherbakov and A. S. Nizamutdinov, Study of Mn^{2+} luminescence in β-PbF_2, *J. Lumin.*, 2019, **194**, 321–326.

5 T. T. Deng, E. H. Song and Y. Y. Zhou, Tailoring photoluminescence stability in double perovskite red phosphors A_2BAlF_6:Mn^{4+} (A = Rb, Cs; B = K, Rb) *via* neighboring-cation modulation, *J. Mater. Chem. C*, 2017, **5**, 12422–12429.

6 D. Yang, L. B. Liao, Q. F. Guo, L. J. Wang, L. F. Mei, H. K. Liu and T. S. Zhou, A novel phosphor of Eu^{3+}-activated Na_3GaF_6: Synthesis, structure, and luminescence properties, *J. Lumin.*, 2019, **194**, 321–326.

7 T. T. Deng, E. H. Song and Y. Y. Zhou, Stable narrowband red phosphor K_3GaF_6:Mn^{4+} derived from hydrous K_2GaF_5 (H_2O) and K_2MnF_6, *J. Mater. Chem. C*, 2017, **5**, 9588–9596.

8 S. K. Saroj, P. Rawat, M. Gupta, G. V. Prakash and R. Nagarajan, Double perovskite K_3InF_6 as upconversion phosphor and its structural transformation by rubidium substitution, *Eur. J. Inorg. Chem.*, 2018, **44**, 4826–4833.

9 J. K. Cao, F. F. Hu, L. P. Chen, H. Guo, C. K. Duan and M. Yin, Wide-range thermometry based on green up-conversion luminescence of K_3LuF_6:Yb^{3+}/Er^{3+} bulk oxyfluoride glass ceramics, *J. Am. Ceram. Soc.*, 2017, **100**, 2108–2114.

10 P. Du and J. S. Yu, Self-activated multicolor emissions in $Ca_2NaZn_2(VO_4)_3$:Eu^{3+} phosphors for simultaneous warm white light-emitting diodes and safety sign, *Dyes Pigm.*, 2017, **147**, 16–23.

11 C. L. Liao, R. P. Cao, W. D. Wang, W. Hu, G. T. Zheng, Z. Y. Luo and P. Liu, Photoluminescence properties and energy transfer of $NaY(MoO_4)_2$:R (R =Sm^{3+}/Bi^{3+}, Tb^{3+}/Bi^{3+}, Sm^{3+}/Tb^{3+}) phosphors, *Mater. Res. Bull.*, 2018, **97**, 490–496.

12 B. Han, Y. Z. Dai, J. Zhang, B. B Liu and H. Z. Shi, Development of near-ultraviolet-excitable single-phase white-light-emitting phosphor $KBaY(BO_3)_2$:Ce^{3+},Dy^{3+} for phosphor-converted white light emitting-diodes, *Ceram. Interfaces*, 2018, **44**, 14803–14810.

13 Q. F. Guo, C. L. Zhao, Z. Q. Jiang, L. B. Liao, H. K. Liu, D. Yang and L. F. Mei, Novel emission-tunable oxyapatites-type phosphors: Synthesis, luminescent properties and the applications in white light emitting diodes with higher color rendering index, *Dyes Pigm.*, 2017, **139**, 361–371.

14 B. Li, X. Y. Huang and J. Lin, Single-phased white-emitting $Ca_3Y(GaO)_3(BO_3)_4$: Ce^{3+},Tb^{3+},Sm^{3+} phosphors with high-efficiency: Photoluminescence, energy transfer and application in near-UV-pumped white LEDs, *J. Lumin.*, 2019, **205**, 115–121.

15 P. L. Li, Z. J. Wang, Q. L. Guo and Z. P. Yang, Luminescence and energy transfer of 432 nm blue LED radiation-converting phosphor $Ca_4Y_6O(SiO_4)_6$: Eu^{2+}, Mn^{2+} for warm white LEDs, *RSC Adv.*, 2015, **5**, 4448–4453.

16 L. Li, X. H. Tang, Z. J. Wu, Y. F. Zheng, S. Jiang, X. Tang, G. T. Xiang and X. J. Zhou, Simultaneously tuning emission color and realizing optical thermometry *via* efficient Tb^{3+}/Eu^{3+} energy transfer in whitlockite-type phosphate multifunctional phosphors, *J. Alloys Compd.*, 2018, **780**, 266–275.

17 Y. L. Zhu, Y. J. Liang, M. F. Zhang, M. H. Tong, G. G. Li and S. Wang, Structure, luminescence properties and energy transfer behavior of color-adjustable $Sr_3Gd_2(Si_3O_9)_2$: Ce^{3+}, Tb^{3+}/Mn^{2+} phosphors, *RSC Adv.*, 2015, **5**, 98350–98360.

18 C. Y. Xu, Y. H. Song, H. X. Guan, Y. Sheng, P. C. Ma, X. Q. Zhou, Z. Shi and H. F. Zou, The photoluminescence, thermal properties and tunable color of $Na_{1-x}Al_{1+2x}Si_{1-2x}O_4$: $xCe^{3+}/Tb^{3+}/Dy^{3+}$ *via* energy transfer: a single-component multicolor-emitting phosphor, *Phys. Chem. Chem. Phys.*, 2017, **19**, 22197–22209.

19 K. Li and R. V. Deun, Photoluminescence and energy transfer properties of a novel molybdate $KBaY(MoO_4)_3$:Ln^{3+} (Ln^{3+} = Tb^{3+}, Eu^{3+}, Sm^{3+}, Tb^{3+}/Eu^{3+}, Tb^{3+}/Sm^{3+}) as a multi-color emitting phosphor for UV w-LEDs, *Dalton Trans.*, 2018, **47**, 6995–7004.

20 M. M. Jiao, Q. F. Xu, M. L. Liu, C. L. Yang and Y. J. Yu, Efficient green phosphor realized by $Ce^{3+}→Tb^{3+}$ energy transfer in $Li_3Sc_2(PO_4)_3$ for ultraviolet white light-emitting diodes, *Phys. Chem. Chem. Phys.*, 2018, **20**, 26995–27002.

21 L. Li, W. X. Chang, W. Y. Chen, Z. S. Feng, C. L. Zhao, P. F. Jiang, Y. J. Wang, X. J. Zhou and A. Suchocki, Double perovskite $LiLaMgWO_6$:Eu^{3+} novel red-emitting phosphors for solid state lighting: Synthesis, structure and photoluminescent properties, *Ceram. Int.*, 2017, **43**, 2720–2729.

22 S. D. Li, Q. Y. Meng, S. C. Lü and W. J. Sun, Study on optical temperature sensing properties of Tb^{3+}, Eu^{3+} co-doped $CaMoO_4$ phosphor, *J. Lumin.*, 2018, **200**, 103–110.

23 X. X. Ma, L. B. Liao, Q. F. Guo, H. K. Liu, T. S. Zhou and L. F. Mei, Luminescence properties and energy transfer investigations of $Ba_2La_{2.85-x}Tb_{0.15}Eu_x(SiO_4)_3F$ multicolor phosphor, *RSC Adv.*, 2018, **8**, 27332–27341.

24 X. M. Zhu and Z. F. Zhou, Photoluminescence and energy transfer mechanism of a novel tunable color phosphor Na_2MgSiO_4:Tb^{3+}, Eu^{3+}, *J. Lumin.*, 2017, **188**, 589–594.

25 S. Lee and S. Park, Preparation and luminescent properties of Tb^{3+} and $Tb^{3+}–Ce^{3+}$ doped $Ba_9Y_2Si_6O_{24}$ phosphors, *J. Lumin.*, 2013, **143**, 215–218.

26 Z. X. Shi, J. Wang and X. Guan, Upconversion multicolor tuning of $NaY(WO_4)_2$:Tb^{3+} with Eu^{3+} doping, *J. Rare Earths*, 2018, **36**, 911–916.

27 M. M. Shang, S. Huang and J. Lin, Multicolor emissions and photoluminescence properties for $Ca_3Al_4ZnO_{10}$:$Ce^{3+}/Eu^{3+}/Tb^{3+}/Mn^{2+}$ phosphors, *J. Lumin.*, 2018, **204**, 493–498.

28 T. A. Safeera and E. I. Anila, An investigation on the luminescence quenching mechanism of $ZnGa_2O_4$:Tb^{3+} phosphor, *J. Lumin.*, 2019, **205**, 277–281.

29 X. Y. Li, X. T. Wei, Y. G. Qin, Y. H. Chen, C. K. Duan and M. Yin, The emission rise time of BaY_2ZnO_5:Eu^{3+} for non-contact luminescence thermometry, *J. Alloys Compd.*, 2016, **657**, 353–357.

30 X. J. Zhou, L. N. Chen, S. Jiang, G. T. Xiang, L. Li, X. Tang, X. B. Luo and Y. Pang, Eu^{3+} activated $LiSrVO_4$ phosphors: Emission color tuning and potential application in temperature sensing, *Dyes Pigm.*, 2018, **151**, 219–226.

31 F. F. Hu, Z. M. Zhao, F. F. Chi, X. T. Wei and M. Yin, Structural characterization and temperature-dependent

luminescence of CaF_2:Tb^{3+}/Eu^{3+} glass ceramics, *J. Rare Earths*, 2017, **35**, 536–541.

32 Z. H. Li, H. Y. Ma, N. Li, Y. Du and Q. Y. Shao, New phosphors of β-BaB_2O_4:RE^{3+} (RE^{3+} = Eu^{3+}, Tb^{3+}), *J. Alloys Compd.*, 2018, **747**, 340–347.

33 L. G. Van Uitert, Characterization of energy transfer interactions between rare earth ions, *J. Electrochem. Soc.*, 1967, **114**, 1048–1053.

34 D. L. Dexter and J. H. Schulman, Theory of Concentration Quenching in Inorganic Phosphors, *J. Chem. Phys.*, 1954, **22**, 1063–1070.

35 X. Zhang, P. He, L. Zhou, J. Shi and M. Gong, Energy transfer and luminescent properties of a green-to-red colour tunable Tb^{3+}, Eu^{3+} co-doped $K_2Y(WO_4)(PO_4)$ phosphor, *Mater. Res. Bull.*, 2014, **60**, 300–307.

36 B. Li, B. Devakumar, L. W. Jin, L. L. Sun and X. Y. Huang, Synthesis, energy transfer and photoluminescence properties of thermal stable multicolour-emitting $Ca_3Gd(AlO)_3(BO_3)_4$: Tb^{3+}, Eu^{3+} phosphors, *J. Lumin.*, 2018, **204**, 386–393.